NUCLEON ELECTROMAGNETIC FORM FACTORS

KEES DE JAGER
Jefferson Lab, 12000 Jefferson Avenue, Newport News Va 23606, USA
E-mail: kees@jlab.org

A review of data on the nucleon electromagnetic form factors in the space-like region is presented. Recent results from experiments using polarized beams and polarized targets or nucleon recoil polarimeters have yielded a significant improvement on the precision of the data obtained with the traditional Rosenbluth separation. Future plans for extended measurements are outlined.

1 Introduction

The nucleon electromagnetic form factors (EMFF) are of fundamental importance for the understanding of their internal structure. These EMFF are generally measured through elastic electron-nucleon scattering. In Plane Wave Born Approximation (PWBA) the cross section can be expressed in terms of the so-called Dirac and Pauli form factors F_1 and F_2, respectively,

$$\frac{d\sigma}{d\Omega} = \sigma_M[(F_1^2 + \kappa^2\tau F_2^2)\cos^2(\frac{\theta_e}{2}) + 2\tau(F_1^2 + \kappa F_2^2)^2\sin^2(\frac{\theta_e}{2})] \qquad (1)$$

where $\tau = Q^2/4(m_N^2)$, Q is the four-momentum transfer, m_N the mass of the nucleon, σ_M the Mott cross section for scattering off a point-like particle, κ the nucleon anomalous magnetic moment, θ_e the electron scattering angle and E_e the electron energy. F_1 parametrizes the distribution of the nucleon charge and of the normal part of the nucleon magnetic moment, F_2 that of the anomalous part of the magnetic moment. These two form factors can be expressed in the so-called electric and magnetic Sachs form factors G_E and G_M, respectively

$$\begin{aligned} G_E &= F_1 - \tau\kappa F_2 \\ G_M &= F_1 + \kappa F_2 \end{aligned} \qquad (2)$$

leading to the so-called Rosenbluth[1] formula

$$\frac{d\sigma}{d\Omega} = \sigma_M[\frac{G_E^2 + \tau G_M^2}{1+\tau} + 2\tau G_M^2\tan^2(\frac{\theta_e}{2})] \qquad (3)$$

This equation shows that G_E and G_M can be determined separately by performing cross-section measurements at fixed Q^2 over a range of (θ_e,E_e) combinations (Rosenbluth separation). In the non-relativistic Breit frame the Sachs form factors can be identified with the Fourier transform of the nucleon charge and magnetization density distributions, such that their derivative at $Q^2 \rightarrow 0$ is related to the charge and magnetization radius, respectively.

Through the middle of the previous decade practically all available proton EMFF data had been collected using the Rosenbluth separation. This experimental procedure requires an accurate knowledge of the electron energy and the total luminosity. In addition, since the contribution to the elastic cross section from the magnetic form factor is weighted with Q^2, data on G_E^p suffer from increasing systematic uncertainties at higher Q^2-values. Data for the neutron resulted mainly from quasi-elastic scattering off the deuteron, because a free neutron target is not available in nature. This additional constraint caused large uncertainties, especially on the data for G_E^n.

These restrictions are clearly presented in the review paper by Bosted *et al.*[2] The then available world data set was compared to the so-called dipole parametrization G_D, which corresponds to exponentially decreasing radial charge and magnetization densities:

$$\begin{aligned} G_D &= \left(\frac{\Lambda^2}{\Lambda^2 + Q^2}\right) \text{ with } \Lambda = 0.84\ GeV/c \text{ and } Q \text{ in } GeV/c \\ G_E^p &= G_M^p \approx \mu_p G_D \\ G_M^n &\approx \mu_n G_D \qquad\qquad G_E^n \approx 0 \end{aligned} \tag{4}$$

Accurate data were available for G_M^p up to Q^2-values of over 20 $(GeV/c)^2$, whereas for G_E^n no significant deviation from zero was measured[44]. For all four EMFF the available data agreed with the dipole parametrization to within 20 %. Both the G_E^p and the G_M^p data could be fitted adequately with an identical parametrization. However, the limitation of the Rosenbluth separation is evident from fig. 1, which shows all available data on G_E^p. Different data sets deviate from each other by up to 50 % at higher Q^2-values, way beyond the already sizeable estimate of the experimental uncertainty.

2 Theory

A frequently used framework[6] to describe the EMFF is that of Vector Meson Dominance (VMD), in which one assumes that the virtual photon - after having become a quark-antiquark pair - couples to the nucleon as a vector meson. The EMFF can then be expressed in terms of coupling strengths

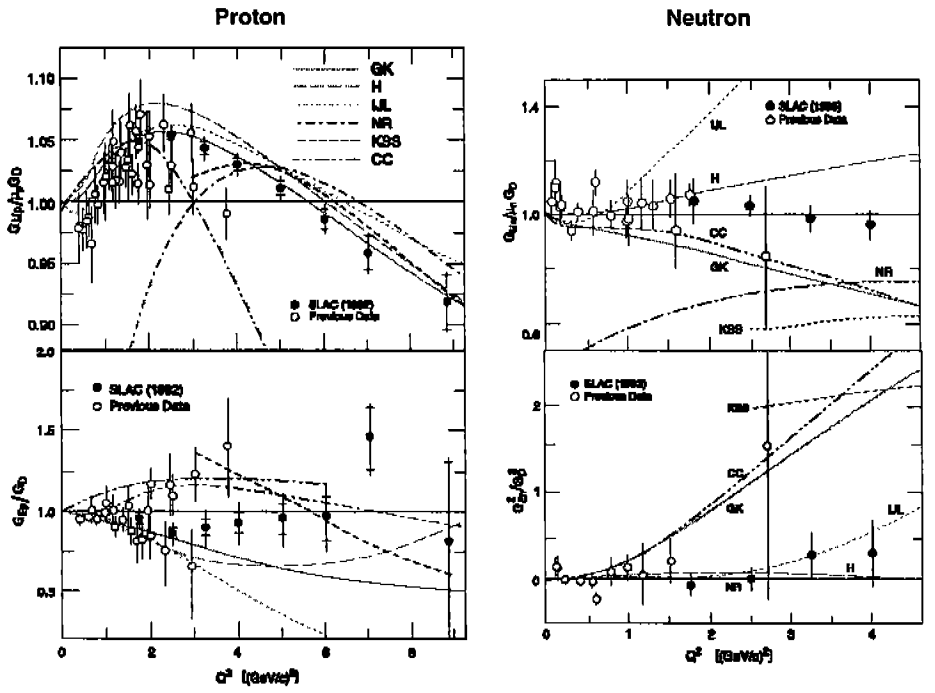

Figure 1. World data on nucleon EMFF available in 1995. The full circles are from ref. [3]. The theory curves are (from the top): GK[5], H[6], IJL[7], NR[8], KSS[9] and CC[10].

between the virtual photon and the vector meson and between the vector meson and the nucleon, summing over all possible vector mesons. In some cases additional terms are included to account for the effect of unknown or lesser known mesons. A common restriction of the VMD models is that they do not predict a correct behaviour of the EMFF at high Q^2-values. The quark-dimensional scaling framework[11] predicts that only valence quark states contribute at sufficiently high Q^2-values. Under these conditions the EMFF Q^2-dependence is determined simply by the number of gluon propagators, causing the Dirac and Pauli form factors to be proportional to Q^{-4} and Q^{-6}, respectively, whereas any VMD-model will predict a Q^{-2} behaviour at large Q^2-values. Gari and Krümpelmann[4,5] have constructed a hybrid (EVMD) model which combines the low Q^2-behaviour of the VMD model with the asymptotic behaviour predicted by pQCD. In their first paper they considered

only coupling to the ρ and ω mesons, whereas later the ϕ meson was also included.

VMD models form a subset of models using dispersion relations, which relate form factors to spectral functions. These spectral functions can also be thought of as a superposition of vector meson poles, but include contributions from n-particle production continua. This framework allows then a model-independent fit[12,13] to all available EMFF data in the space- and the time-like region.

Many attempts have been made to enlarge the domain of applicability of pQCD calculations to moderate Q^2-values. Kroll *et al.*[9] have generalized the hard-scattering scheme by assuming nucleons to consist of quarks and diquarks. The diquarks are used to approximate the effects of correlations in the nucleon wave function. This model is equivalent to the hard-scattering formalism of pQCD in the limit $Q^2 \to \infty$. Chung and Coester[10] have developed a relativistic constituent quark model with effective quark masses and a confinement scale as free parameters. Lu *et al.*[15] have recently expanded the cloudy bag model, whereby the nucleon is described as a bag containing three quarks, by including an elementary pion field coupled to them, in such a way that chiral symmetry is restored. As mentioned earlier, Brodsky and Farrar[11] had shown that in the pQCD limit the ratio F_2/F_1 is proportional to Q^{-2}. Recently, Ralston *et al.*[16] predicted this ratio to scale with Q^{-1} if they assumed the contributions to the proton wavefunction from the quark angular momentum $L_q = 0$ or 1 to be equal.

Recent developments[17] within the Generalized Parton Distribution formalism indicate a relation between the EMFF behaviour at larger Q^2-values and the nucleon spin. One should keep in mind, however, that all presently available theories are at least to some extent effective (or parametrizations). Only lattice QCD theory could provide a truely ab initio calculation, but reliable results for the EMFF are still several years away.

3 Polarization Instrumentation

Over 20 years ago Akhiezer and Rekalo[25] and Arnold *et al.*[26] showed that the accuracy of EMFF measurements could be increased significantly by scattering polarized electrons off a polarized target (or by equivalently measuring the polarization of the recoiling nucleon). In the early nineties a series of measurements[45,46,47,48,35,36] at the MIT-Bates facility showed the feasibility of that measurement principle, as demonstarted in figs. 2 and 3.

Since then, significant technological advances have resulted in a large number of new data with a significantly improved accuracy. Polarized elec-

tron beams[27,28] are now reliably available with a polarization in excess of 80 % at currents of up to 100 μA. The beam polarization is measured with either Møller[29] or Compton[30] polarimeters with an accuracy approaching 1 %. Dynamically polarized targets[31] provide polarized hydrogen or deuterium targets with an average polarization of 80, resp. 20 %, while polarized helium targets are available with a polarization close to 50 % at a density of 10 atm, either through spin[32] or metastability[33] exchange. Finally, the polarization of recoiling or knocked-out reaction products can be measured with focal-plane[34] or neutron[54] polarimeters.

4 Neutron Magnetic Form Factor

Significant progress has been made in measurements of G_M^n at low Q^2-values by measuring the ratio of quasi-elastic neutron and proton knock-out from a deuterium target. This method is practically insensitive to nuclear binding effects and to fluctuations in the luminosity and detector acceptance. The basic set-up used in all such measurements was very similar: the electron was detected in a magnetic spectrometer with coincident neutron/proton detection in a large scintillator array. The main technical difficulty in such a ratio measurement is the absolute determination of the neutron detection efficiency. For the measurements at Bates[36] and ELSA[37] the efficiency was measured in situ using the $D(\gamma,p)n$ or the $p(\gamma,\pi^+)$ reaction with a bremsstrahlung radiator up stream of the experimental target. The hadron detectors used in the experiments at NIKHEF[39] and Mainz[40,41] were calibrated at the PSI neutron beam using the kinematically complete $p(n,p)n$ reaction. Figure 2 shows the results of those four experiments. The Mainz G_M^n data are 8-10 % lower than those from ELSA, at variance with the quoted uncertainty of appr. 2 %. This discrepancy would require a 16-20 % error in the detector efficiency. The contribution from electroproduction in the ELSA set-up, caused by the electron contamination in the bremsstrahlung beam, which could result in a loss of events due to the three-body kinematics in electroproduction, has been extensively investigated[38]. Thus far, the detection inefficiency due to electroproduction has been established at less than 5 %, clearly much smaller than required to explain the discrepancy in the data.

The high accuracy of the Mainz data set by itself has allowed to extract a precise value of the magnetic radius of the neutron $< r_M^2 >_n^{1/2} = 0.89 \pm 0.07\ fm$, in excellent agreement with the proton charge and magnetic radius values 0.86 ± 0.01 and $0.86 \pm 0.06\ fm$, respectively.

None of the available theoretical predictions[12,14,15,22] shown in fig. 2 provides an accurate description of the data. The dispersion theory of Mergell

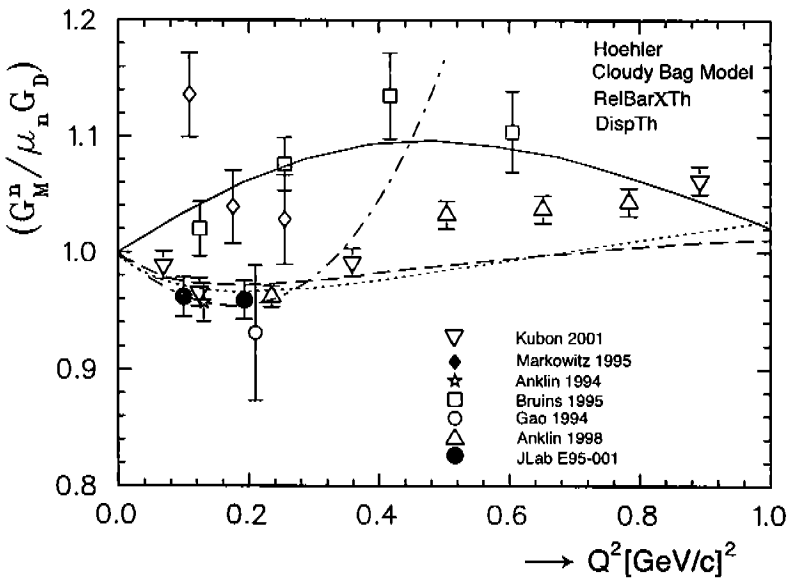

Figure 2. The neutron magnetic form factor G_M^n, in units of the dipole parametrization μG_D, as a function of Q^2. The data are from refs.[41,36,39,37,35,40,42]. The theory curves are dotted[6], dashed[12], dot-dashed[14] and solid[15].

et al.[12] and the old VMD prediction of Höhler *et al.*[6] are in reasonable agreement with the general trend of the data from Mainz.

Recently, inclusive quasi-elastic scattering of polarized electrons off a polarized ^3He target was measured[42] in Hall A at JLab in a Q^2-range from 0.1 to 0.6 $(GeV/c)^2$. This experiment has provided an independent accurate measurement of G_M^n at Q^2-values of 0.1 and 0.2 $(GeV/c)^2$, in excellent agreement with the Mainz data. At the higher Q^2-values the nuclear medium corrections[23,24] have not yet been expanded with relativistic effects. A study of G_M^n at Q^2-values up to 5 $(GeV/c)^2$ has recently been completed at JLab by measuring the neutron/proton quasi-elastic cross-section ratio using the CLAS detector[43].

5 Neutron Electric Form Factor

Since a free neutron target is not available, one has to use neutrons bound in nuclei to study the neutron EMFF. The most precise data on G_E^n prior

to any spin-dependent experiment were obtained from the elastic electron-deuteron scattering experiment by Platchkov *et al.*[49] The deuteron elastic form factor $A(Q^2)$ contains a term of the form $G_E^n G_E^p$. However, in order to extract G_E^n from the data, one has to calculate the deuteron wave function, which requires a choice of the nucleon-nucleon potential. Figure 3 shows the values extracted from the Platchkov data with the Paris potential, while the grey band indicates the range of G_E^n-values extracted with the Nijmegen, AV14 and RSC potentials. Evidently, the choice of NN-potentials results in a systematic uncertainty of appr. 50 % in G_E^n. Recently, Schiavilla and Sick[50] have extracted G_E^n from the data available on the quadrupole form factor G_Q of the deuteron (by combining data on A, B and T_{20}). The results shown in fig. 3 indicate that the model dependence in G_E^n extracted from G_Q is significantly smaller than from A.

In the last decade a series of spin-dependent measurements have provided new accurate data on G_E^n, by utilizing the fact that the ratio of the beam-target asymmetry with the target polarization perpendicular and parallel to the momentum transfer is directly proportional to the ratio of the electric and magnetic form factors:

$$\frac{G_E^n}{G_M^n} = \frac{A_\perp}{A_{//}} \sqrt{\tau + \tau\,(1+\tau)\tan^2(\theta_e/2)} \qquad (5)$$

A similar relation can be derived for the reaction ${}^2H(\vec{e}, e'\vec{n})$ when one measures the polarization of the recoiling neutron directly and after having precessed the neutron spin over 90^o with a dipole magnet.

Figure 3 shows results, obtained through the reaction channels ${}^2\vec{H}(\vec{e}, e'n)$[52], ${}^2H(\vec{e}, e'\vec{n})$[53,54] and ${}^3\vec{H}e(\vec{e}, e'n)$[55,56]. At low Q^2-values corrections for nuclear medium and rescattering effects can be sizeable: 65 % for ${}^2H$ at 0.15 $(GeV/c)^2$ and 50 % for ${}^3\vec{H}e$[23] at 0.35 $(GeV/c)^2$. These corrections are expected to decrease significantly with increasing Q, although no reliable results are at present available for ${}^3\vec{H}e$ above 0.5 $(GeV/c)^2$. Thus, there are now data from a variety of reaction channels available in a Q^2-range up to 0.6 $(GeV/c)^2$ with an overall accuracy of appr. 20 %, which are in mutual agreement. However, neither the VMD[4] nor the dispersion relation[14] calculation agrees with the data. Only the Galster parametrization[57] which uses a modified version of the dipole form factor, is able to describe the data adequately.

Also shown in fig. 3 are the results expected in the near future, from the ${}^2\vec{H}(\vec{e}, e'n)$[62] and ${}^2H(\vec{e}, e'\vec{n})$[60] channels at JLab and from the ${}^2H(\vec{e}, e'\vec{n})$[58] channel at Mainz. Recently an experiment[63] has been approved at JLab to

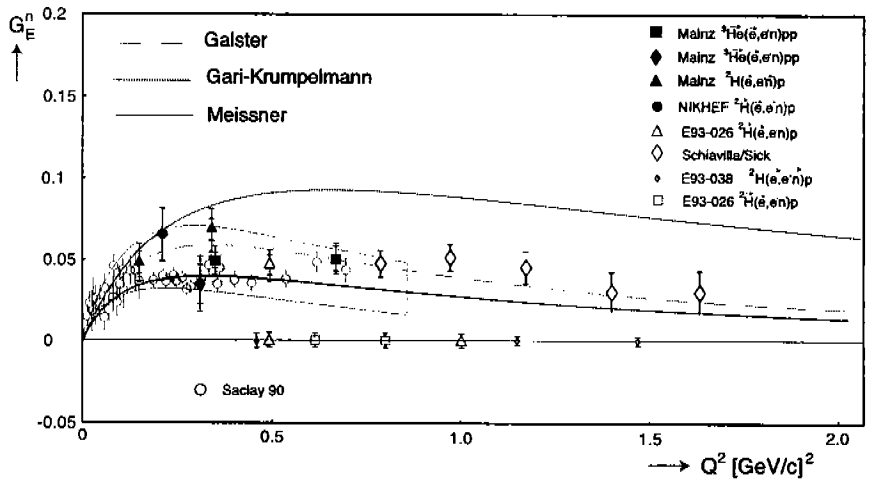

Figure 3. The neutron electric form factor G_E^n as a function of Q^2. The data are indicated by the following symbols: solid - squares[55,56], diamonds[51], triangles[53,54], and circle[52], open - circles[49], triangle[59], diamonds[50] - and small diamonds[60]. Theory curves are dotted[14] and solid[5], while the Galster parametrization[57] is presented by the dashed curve. Symbols on the zero axis indicate the Q^2-value and the size of the error bars of ongoing experiments[60,?].

measure G_E^n at Q^2-values of 2.4 and 3.4 $(GeV/c)^2$ using the $^3\vec{H}e(\vec{e},e'n)$ reaction. The BLAST facility[61] at MIT is expected to provide highly accurate data on G_E^n in a Q^2-range from 0.1 to 0.8 $(GeV/c)^2$. Thus, within a couple of years G_E^n data with an accuracy of 10 % or better will be available up to a Q^2-value of 3.4 $(GeV/c)^2$.

6 Proton Electric Form Factor

Arnold *et al.*[26] have shown that the systematic error in a measurement of G_E^p, inherent to the Rosenbluth separation, can be significantly reduced by scattering longitudinally polarized electrons off a hydrogen target and measuring the ratio of the transverse to longitudinal polarization of the recoiling proton.

$$\frac{G_E^p}{G_M^p} = -\frac{P_t}{P_l}\frac{E_e + E_e}{2m_N}\tan\left(\frac{\theta_e}{2}\right) \tag{6}$$

This ratio of the two polarization components P_t and P_l can be measured

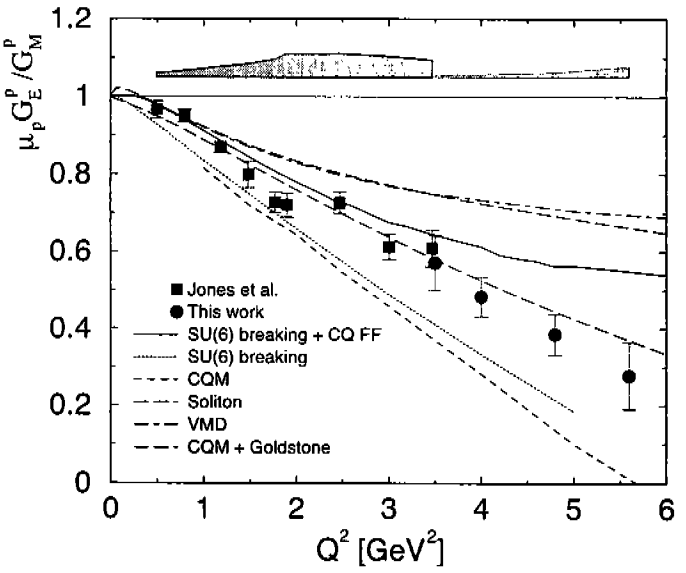

Figure 4. The ratio $\mu G_E^p/G_M^p$ from ref.[66](open squares) and ref.[67](solid circles), compared to various theoretical calculations: dash-dotted[13], thin dashed[19], solid[18], dashed[20], dotted[18] and short dashed[21]. The systematic errors for both experiments are shown as a band at the top of the figure.

in a focal plane polarimeter, while neither the beam polarization nor the polarimeter analyzing power need be known. This method was first used by Milbrath *et al.*[64] at MIT-Bates to measure the ratio G_E^p/G_M^p at low Q^2.

This technique has been used in two experiments[66,67], performed in Hall A at JLab, to measure the ratio G_E^p/G_M^p in a Q^2-range from 0.5 to 5.6 $(GeV/c)^2$. Longitudinally polarized electrons, with a polarization of up to 70 % and energies between 0.9 and 4.6 GeV were scattered in a 15 cm long liquid hydrogen target. Elastic *ep* events were selected by detecting electrons and protons in coincidence in the two identical HRS spectrometers. At the four highest Q^2-values a lead-glass calorimeter was used to detect the scattered electrons. The polarization of the recoiling proton was determined with a Focal Plane Polarimeter (FPP) in the hadron HRS, consisting of two pairs of straw chambers with a carbon (or polyethylene) analyzer in between. Instrumental asymmetries are cancelled by taking the difference of the azimuthal distributions of the protons scattered in the analyzer for positive and negative beam helicity.

A Fourier analysis of this difference then yields the transverse and normal polarization components at the FPP. The data were analyzed in bins of each of the target coordinates. No dependence on any of these variables was observed. The results for the ratio G_E^p/G_M^p are shown in fig. 4. The most striking feature of the data is the sharp decline as Q^2 increases. Since it is known that G_M^p closely follows the dipole parametrization, it follows that G_E^p falls more rapidly with Q^2 than the dipole form factor G_D. A comparison with fig. 1 confirms the expected improvement in accuracy of such a spin-dependent measurement over the Rosenbluth separation. All theoretical calculations shown in fig. 4 predict a gradual decrease of G_E^p. The prediction by Holzwarth[20], who used a relativistic chiral soliton model, provides the best agreement with the data. At the highest Q^2-values the data do not follow pQCD scaling[11], but rather the $1/Q$ behaviour in F_2/F_1, predicted by Ralston *et al.*[16]. If one assumes the linear decrease in G_E^p/G_M^p to continue, G_E^p would cross zero at $Q^2 \approx 7.7\ (GeV/c)^2$. To investigate this possibility an extension[68] of this experiment to a Q^2-value of 9.6 $(GeV/c)^2$ has been approved to run in Hall C.

The symmetric arrangement of the detector segments of BLAST[61] allows a simultaneous measurement of a cross-section asymmetry at different Q^2-values. This technique will provide data on G_E^p with an unprecedented accuracy of ≈ 0.3 % in a Q^2-range from 0.07 to 0.9 $(GeV/c)^2$[69].

7 Proton Magnetic Form Factor

No new data have become available on the magnetic form factor of the proton G_M^p since ref.[3]. Brash *et al.*[70] have reanalyzed the world data set on G_M^p imposing the form factor ratio G_E^p/G_M^p as measured in refs.[66,67] as a constraint. As a result the data lie appr. 2 % higher than the original parametrization of Bosted *et al.*[2]

8 Summary

Recent advances in polarized electron sources, polarized nucleon targets and nucleon recoil polarimeters have made it possible to accurately measure the spin-dependent elastic electron-nucleon cross section. New data on nucleon electro-magnetic form factors with an unprecedented precision have (and will continue to) become available in an ever increasing Q^2-domain. These data will form tight constraints on models of nucleon structure and will hopefully incite new theoretical efforts. In addition they will significantly improve the accuracy of the extraction of strange form factors from parity-violating experiments.

26. R. Arnold, C. Carlson and F. Gross, *Phys. Rev.* C **23**, 363 (1981).
27. K. Aulenbacher *et al.*, *Nucl. Instrum. Methods* A **391**, 498 (1997).
28. M. Poelker *et al.*, Proc. of the 14th Int. Symp. on High-Energy Spin Physics, Osaka (2000), p. 943.
29. M. Hauger *et al.*, *Nucl. Instrum. Methods* A **462**, 382 (2001).
30. N. Falletto *et al.*, *Nucl. Instrum. Methods* A **459**, 412 (2001).
31. D. Crabb and D. Day *et al.*, *Nucl. Instrum. Methods* A **356**, 9 (1995); T.D. Averett *et al.*, *Nucl. Instrum. Methods* A **427**, 440 (1999).
32. P.L. Anthony *et al.*, *Phys. Rev. Lett.* **71**, 959 (1993); *Phys. Rev.* D **54**, 6620 (1996); J.S. Jensen, Ph.D. Thesis, CalTech, 2000 (unpublished).
33. R. Surkau *et al.*, *Nucl. Instrum. Methods* A **384**, 444 (1997).
34. M.K. Jones *et al.*, AIP Conf. Proc. 412, ed. T.W. Donnelly, p. 342 (1997); L. Bimbot *et al.*, to be submitted to *Nucl. Instr. Meth.*
35. H. Gao *et al.*, *Phys. Rev.* C **50**, R546 (1994).
36. P. Markowitz *et al.*, *Phys. Rev.* C **48**, R5 (1993).
37. E.E.W. Bruins *et al.*, *Phys. Rev. Lett.* **75**, 21 (1995).
38. B. Schoch, private communication (1999).
39. H. Anklin *et al.*, *Phys. Lett.* B **336**, 313 (1994).
40. H. Anklin *et al.*, *Phys. Lett.* B **428**, 248 (1998).
41. G. Kubon *et al.*, *Phys. Lett.* B **524**, 26 (2002).
42. W. Xu *et al.*, *Phys. Rev. Lett.* **85**, 2900 (2000).
43. W. Brooks and M.F. Vineyard, JLab experiment E94-017.
44. A.F. Lung *et al.*, *Phys. Rev. Lett.* **70**, 718 (1993).
45. T. Eden *et al.*, *Phys. Rev.* C **50**, R1749 (1994).
46. C.E. Woodward *et al.*, *Phys. Rev. Lett.* **65**, 698 (1990).
47. C.E. Jones-Woodward *et al.*, *Phys. Rev.* C **44**, R571 (1991).
48. A.K. Thompson *et al.*, *Phys. Rev. Lett.* **68**, 2901 (1992).
49. S. Platchkov *et al.*, *Nucl. Phys.* A **510**, 740 (1990).
50. R. Schiavilla and I. Sick, *Phys. Rev.* C **64**, 041002 (2001).
51. M. Meyerhoff *et al.*, *Phys. Lett.* B **327**, 201 (1994).
52. I. Passchier *et al.*, *Phys. Rev. Lett.* **82**, 4988 (1999).
53. C. Herberg *et al.*, *Eur. Phys. Jour.* A **5**, 131 (1999).
54. M. Ostrick *et al.*, *Phys. Rev. Lett.* **83**, 276 (1999).
55. J. Becker *et al.*, *Eur. Phys. Jour.* A **6**, 329 (1999).
56. D. Rohe *et al.*, *Phys. Rev. Lett.* **83**, 4257 (1999).
57. S. Galster *et al.*, *Nucl. Phys.* B **32**, 221 (1971).
58. H. Schmieden *et al.*, MAMI proposal A1/2-99.
59. H. Zhu *et al.*, *Phys. Rev. Lett.* **87**, 081801 (2001).
60. B.D. Anderson, S. Kowalski and R. Madey, JLab experiment E93-038.
61. Bates Large Acceptance Spectrometer Toroid, http://mitbates.mit.edu

/blast.
62. D. Day, JLab proposal E93-026.
63. B. Wojtsekhowski *et al.*, JLab proposal E02-013.
64. B. Milbrath *et al.*, *Phys. Rev. Lett.* **80**, 452 (1998); erratum, *Phys. Rev. Lett.* **82**, 2221 (1999).
65. T. Pospischil *et al.*, *Eur. Phys. Jour.* A **12**, 125 (2001).
66. M.K. Jones *et al.*, *Phys. Rev. Lett.* **84**, 1398 (2000).
67. O. Gayou *et al.*, accepted for *Phys. Rev. Lett.*
68. C.F. Perdrisat *et al.*, JLab experiment E01-109.
69. H. Gao, J.R. Calarco and H. Kolster, MIT-Bates proposal 01-01.
70. E. Brash *et al.*, hep-ex/0111038.